

Large is different: non-monotonic behaviour of elastic range scaling in polymeric turbulence at large Reynolds and Deborah numbers

Marco E. Rosti,^{1,*} Prasad Perlekar,² and Dhrubaditya Mitra³

¹*Complex Fluids and Flows Unit, Okinawa Institute of Science and Technology Graduate University, 1919-1 Tancha, Onna-son, Okinawa 904-0495, Japan*

²*TIFR Centre for Interdisciplinary Sciences, Tata Institute of Fundamental Research, Gopanpally, Hyderabad 500046, India.*

³*Nordita, KTH Royal Institute of Technology and Stockholm University, Roslagstullsbacken 23, 10691 Stockholm, Sweden*

We use direct numerical simulations to study homogeneous, and isotropic turbulent flows of dilute polymer solutions at high Reynolds and Deborah numbers. We find that for small wavenumbers k , the kinetic energy spectrum shows Kolmogorov-like behavior which crosses over at a larger k to a novel, elastic scaling regime, $E(k) \sim k^{-\xi}$, with $\xi \approx 2.3$. We study the contribution of the polymers to the flux of kinetic energy through scales, and find that it can be decomposed into two parts: one increase in effective viscous dissipation, and a purely elastic contribution that dominates over the nonlinear flux in the range of k over which the elastic scaling is observed. The multiscale balance between the two fluxes determines the crossover wavenumber which depends non-monotonically on the Deborah number. Consistently, structure functions also show two scaling ranges, with intermittency present in both of them in equal measure.

I. INTRODUCTION

Since the discovery of turbulent drag reduction by Toms [2], turbulent flows with small amount of long-chained polymers have remained an exciting field of research. In addition to polymer concentration, two dimensionless numbers, the Reynolds number and the Deborah number, are necessary to describe such a turbulent flow. The former estimates the importance of the inertial term in the Navier–Stokes equation compared to the viscous term, and the latter is the ratio of the characteristic time scale of the polymers over the typical time scale of the large scale eddies in the turbulent flow. The turbulent drag reduction appears at both large Reynolds and Deborah numbers. Evidently, it is not possible to study drag reduction in homogeneous and isotropic turbulent flows, nevertheless such flows are studied, since the pioneering work by Tabor and De Gennes [3], in search of deeper insights.

The elementary effect of the addition of polymers to a fluid is an increase in the effective viscosity of the solution [4, 5]. Nevertheless, there can be net reduction of the dissipation of kinetic energy [6–12] because the presence of polymers changes the turbulent cascade *qualitatively*. Significant theoretical [3, 5, 13–15], numerical [9, 11, 12, 16–27], and experimental [1, 6, 28–33] efforts have gone into elucidating the nature of the turbulent energy cascade in the presence of polymers. It is now reasonably well established [9, 11] that for large enough scale separation between the energy injection scale, L_{inj} , and the Kolmogorov scale, L_K , there exists an intermediate scale L_p such that for scales $L_p < r < L_{\text{inj}}$ the energy cascade is practically the same as that of a Newtonian flow, with the the second order structure function $S_2(r) \sim r^{2/3}$ and the shell-integrated energy spectrum being $E(k) \sim k^{-5/3}$. For scales r in the range $L_K < r < L_p$, energy is transferred from the fluid to the polymers and the kinetic energy spectrum is steeper than the Kolmogorov spectrum or in other words the second order structure function increases faster with r than $r^{2/3}$. Using the concept of scale-dependent Reynolds number [34], we may identify the flow at scale $r < L_p$ (also valid for $r < L_K$) with elastic turbulence – random viscoelastic smooth flows at very small Reynolds number. The spectrum for elastic turbulence is expected to be $E(k) \sim k^{-\xi}$ with $\xi > 3$ [15, 35, 36]. Is there a new scaling range for $r < L_p$ over which $S_2(r) \sim r^{\zeta_2}$ with $2/3 < \zeta_2 < 2$? This question could not be probed with the low-Reynolds and low-Deborah simulations quoted above. Recent experiments [1] had tentatively suggested that a new scaling range indeed appears, although the evidence is not yet unequivocal. Experiments [1, 37] also showed that, contrary to Lumley’s arguments [38], the scale L_p does depends on the concentration of polymers.

Here we present evidence, from the highest resolution 3D simulations of polymeric fluids, that indeed there is a range of scales r over which the structure function $S_2(r)$ seems to show scaling consistent with recent experimental results [1]. We also show that the new scaling is a purely elastic effect, and that this elastic behaviour is non-monotonic in the Deborah number.

* marco.rosti@oist.jp

II. RESULTS

A. Governing equations

We use direct numerical simulations to study three dimensional homogeneous isotropic turbulence with polymers [4, 39–43]. These are represented by a second rank tensor, \mathcal{C} with components $C_{\alpha\beta}$, which emerges as the thermal average of the tensor-product of the polymer end-to-end distance with itself. The polymer molecules are assumed to have a single relaxation time τ_p . The dynamical equations are:

$$\rho_f \left(\frac{\partial u_\alpha}{\partial t} + \frac{\partial u_\alpha u_\beta}{\partial x_\beta} \right) = -\frac{\partial p}{\partial x_\alpha} + \frac{\partial}{\partial x_\beta} \left(2\mu_f S_{\alpha\beta} + \frac{\mu_p}{\tau_p} f C_{\alpha\beta} \right) + F_\alpha, \quad (1a)$$

$$\frac{\partial C_{\alpha\beta}}{\partial t} + u_\gamma \frac{\partial C_{\alpha\beta}}{\partial x_\gamma} = C_{\alpha\gamma} \frac{\partial u_\beta}{\partial x_\gamma} + C_{\gamma\beta} \frac{\partial u_\alpha}{\partial x_\gamma} - \frac{f C_{\alpha\beta} - \delta_{\alpha\beta}}{\tau_p}, \quad (1b)$$

$$\frac{\partial u_\alpha}{\partial x_\alpha} = 0. \quad (1c)$$

Here u_α is the velocity, $\rho_f = 1$ and μ_f are the density and dynamic viscosity of the fluid, p is the pressure, μ_p is the polymer viscosity, and \mathcal{S} is the rate-of-strain tensor with components $S_{\alpha\beta}$ defined as $S_{\alpha\beta} = (\partial u_\alpha / \partial x_\beta + \partial u_\beta / \partial x_\alpha) / 2$. The function f is equal to unity ($f = 1$) in the purely elastic Oldroyd-B model, and to $f = (\mathcal{L}^2 - 3) / (\mathcal{L}^2 - C_{\gamma\gamma})$ in the FENE-P model (where \mathcal{L} is the maximum allowed extension of the polymers) exhibiting both shear-thinning and elasticity. The polymer timescale is the relaxation time τ_p and its concentration is related to the value of $1 + \mu_p / \mu_f$; the value chosen in this work corresponds, roughly, to 100 ppm for polyethylene oxide [44]. Note that, we work in the dilute limit where polymer concentration is assumed to be homogeneous. Turbulence is sustained by the external force in the momentum equation, F ; we use the spectral scheme from Eswaran and Pope [45] to randomly inject energy to the low-wavenumber shells with $k_{\text{inj}} = (1 \leq k \leq 2)$. Note that, the scaling behavior in wavenumbers much larger than k_{inj} are independent of the choice of k_{inj} . In the statistically stationary state of turbulence, the injected energy is dissipated by both the fluid (ε_f) and the polymers (ε_p), thus $\varepsilon_{\text{inj}} = \varepsilon_f + \varepsilon_p$, where

$$\varepsilon_f = \frac{2\mu_f}{\rho_f} \langle S_{\alpha\beta} S_{\alpha\beta} \rangle, \quad \varepsilon_p = \frac{\mu_p}{2\rho_f \tau_p^2} \langle f (f C_{\mu\mu} - 3) \rangle. \quad (2)$$

To compare, we also solve for the Navier–Stokes equations without any polymer additive – we call this the Newtonian simulation.

B. Theoretical background

Let us briefly recall essential features of fluid turbulence without polymeric additives [46]. The flow is determined by one dimensionless number, $\text{Re} = u_{\text{rms}} / (k_{\text{inj}} \nu_f)$, where u_{rms} is the root-mean-square velocity and $\nu_f = \mu_f / \rho_f$ is the kinematic viscosity of the fluid. Turbulent flows possess a range of length scales and corresponding time scales. The statistical properties of such flows are characterized by the scaling exponents, ζ_q of the q -th order longitudinal structure functions, S_q , defined by:

$$S_q(\ell) = \langle \delta u(\ell)^q \rangle \sim \ell^{\zeta_q} \quad \text{where} \quad (3a)$$

$$\delta u(\ell) \equiv [u(x + \ell) - u(x)] \cdot \left(\frac{\ell}{L} \right). \quad (3b)$$

Here $\langle \cdot \rangle$ denotes averaging over the statistically stationary state of turbulence. The q -th order structure function is the q -th order moment of the probability distribution function of velocity difference across a length scale ℓ . The scaling behavior of the structure function, (3a), holds for $\eta \ll \ell \ll L$ where $\eta \equiv (\nu_f^3 / \varepsilon_{\text{inj}})^{1/4}$ is called the viscous scale and L is called the integral scale. In practice, $L = 2\pi / k_L$ is of the same order of $L_{\text{inj}} = 2\pi / k_{\text{inj}}$ and we will use them interchangeably.

The shell-integrated energy spectrum in Fourier space

$$E(k) \equiv \int_{|m|=k} d^3m \langle \hat{u}(m) \hat{u}(-m) \rangle, \quad (4)$$

where $\hat{u}(m)$ is the Fourier transform of the velocity field $u(x)$, is itself the Fourier transform of the second order structure function $S_2(\ell)$. The theory of Kolmogorov gives $\zeta_q = q/3$ and consequently $E(k) \sim k^{-5/3}$, when k lies

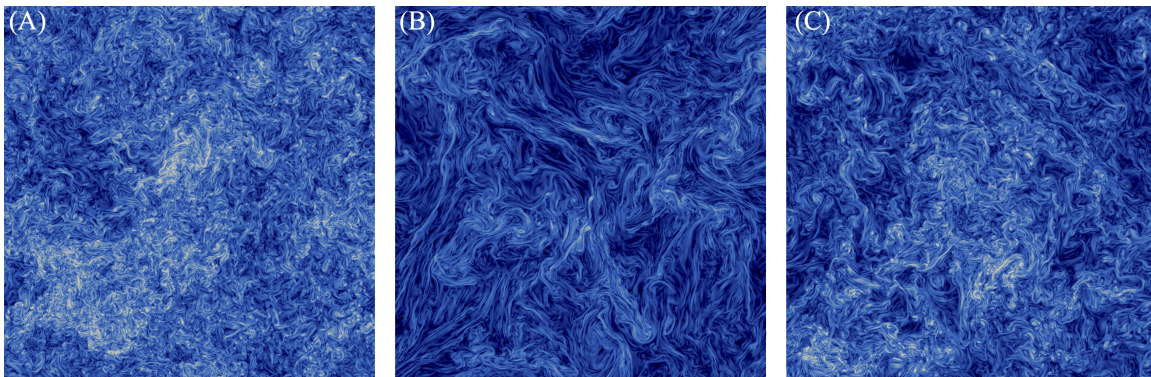


FIG. 1. **Instantaneous snapshots of the turbulent flows.** (A) Newtonian and viscoelastic fluid with (B) $De \approx 1$ and (C) $De \approx 25$, at a nominal microscale Reynolds number $Re_\lambda \approx 400$ for the Newtonian case ((A): $Re_\lambda = 390$, (B) $Re_\lambda \approx 740$, (C) $Re_\lambda \approx 447$). The color contour shows the magnitude of the vorticity field, with the color-scale going from 0 (blue) to the maximum (white). The figures are two-dimensional cuts of the three-dimensional periodic cube passing through the middle of the domain.

within the *inertial range*, $k_{inj} \ll k \ll k_\eta$, with $k_\eta \sim 1/\eta$. The turbulent velocity fluctuations are non-Gaussian in two ways. First, the odd-order structure functions are non-zero, in particular the third order structure function satisfies the most celebrated exact relation in turbulence, i.e. the four-fifth law, $S_3(\ell) = -(4/5)\varepsilon_{inj}\ell$ – this result is the cornerstone of Kolmogorov’s theory of turbulence. Second, the scaling exponents ζ_q are a nonlinear convex function of q – a phenomena called *intermittency*.

In the presence of polymers, we, in addition, consider

$$E_p(k) \equiv \left(\frac{\mu_p}{\rho_f \tau_p} \right) \int_{|m|=k} d^3m \left\langle \hat{B}_{\gamma\beta}(m) \hat{B}_{\beta\gamma}(-m) \right\rangle, \quad (5)$$

where the matrix \mathcal{B} with components, $B_{\alpha\gamma}$, is the (unique) positive symmetric square root of the matrix \mathcal{C} , i.e., $C_{\alpha\beta} = B_{\alpha\gamma} B_{\gamma\beta}$ [25, 48]. For the Oldroyd-B model the total energy in the polymeric mode is given by

$$\mathcal{E}_p \equiv \frac{1}{2} \int dk E_p(k) = \frac{\mu_p}{2\rho_f \tau_p} \langle C_{\mu\mu} \rangle. \quad (6)$$

The presence of polymers introduces also a new dimensionless number which is the ratio of the polymeric time scale τ_p over a characteristic time scale of the flow. As the turbulent flow has many time scales, it is common to define the Deborah number $De \equiv \tau_p/\tau_L$, where $\tau_L = L/u_{rms}$ is the large-eddy-turnover-time, and the Weissenberg number $Wi \equiv \tau_p/\tau_\eta$, where $\tau_\eta = \eta^2/\nu$ [49].

In Fig. (1) we show typical pseudocolor plots of vorticity from Newtonian and viscoelastic simulations. The flow is qualitatively strongly affected by the presence of polymers, and small-scale vorticity structures are smoothed out by the presence of the polymers, as can be seen by comparing Fig. (1A) and Fig. (1B), see also Ref. [9, 11, 18]. Surprisingly, as the Deborah number is increased beyond unity, this qualitative trend is reversed, compare Fig. (1B) and Fig. (1C). In Fig. (1C) small scale structures in vorticity reappears but at the same time we still find elongated structures although their length scales are smaller than their counterparts in Fig. (1B).

C. Kinetic and polymer energy spectra

In Fig. (2) we plot the turbulent kinetic energy $E(k)$ for several values of Deborah number De . For the small Deborah numbers, e.g. $De \approx 0.18$, we observe, practically, the same behavior as Kolmogorov turbulence, with $E(k) \sim k^{-5/3}$ for the inertial range. As the Deborah number increases the range over which the Kolmogorov scaling is valid shrinks to smaller k , and at intermediate k a new range over which $E(k) \sim k^{-\xi}$ with $\xi \approx 2.3$ emerges. We call this new scaling range the *elastic range*. The spectra, in general, has three characteristic length scales (or equivalently wavenumbers). The largest is the one where energy is injected by stirring, the integral scale, $L \approx L_{inj}$. Next is the scale at which the Kolmogorov scaling crosses over to elastic scaling, L_p (corresponding wavenumber $k_p = 2\pi/L_p$). Last is the scale at which elastic scaling crosses over to the dissipative range, which we call the dissipative scale η (corresponding wavenumber $k_\eta = 1/\eta$). The Kolmogorov scaling is observed over the range $k_{inj} < k < k_p$ and the elastic range

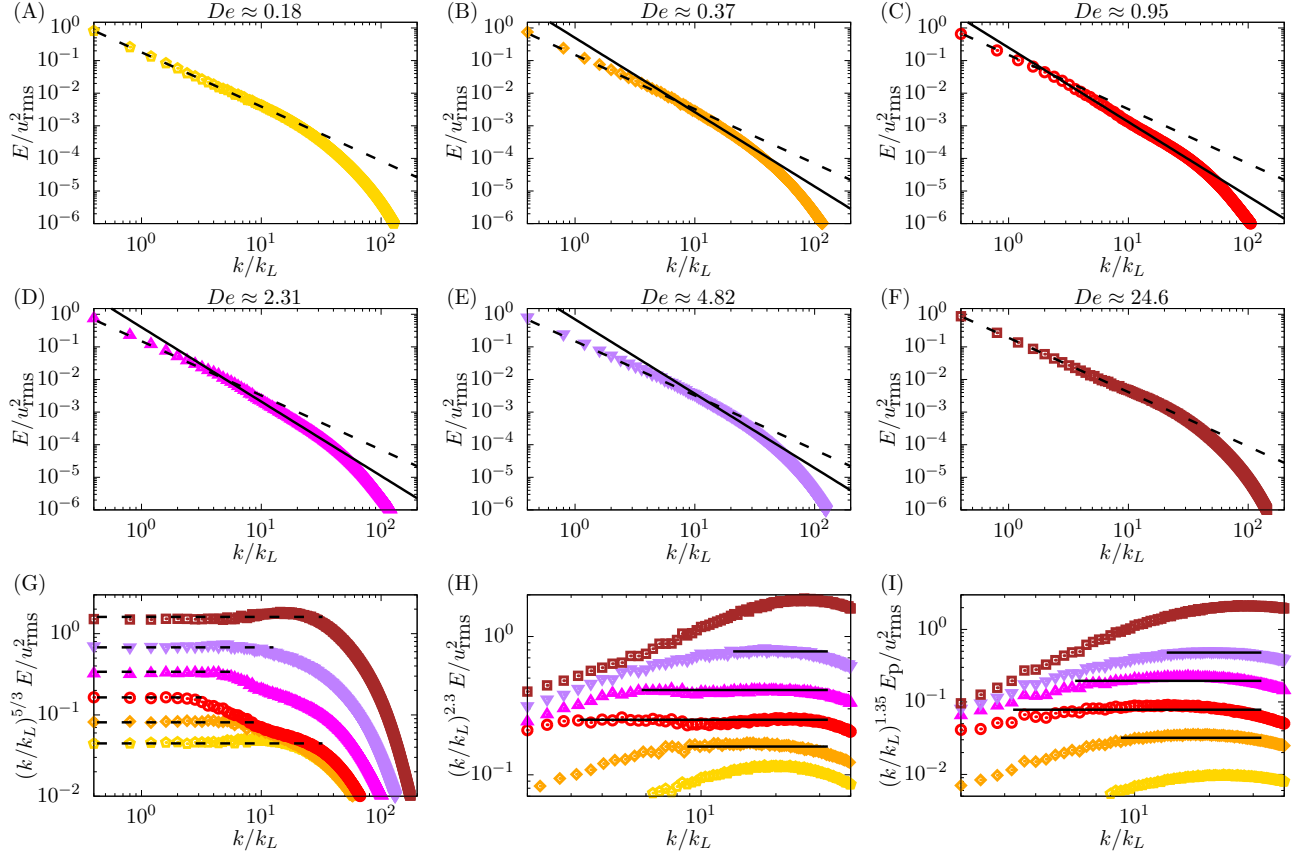


FIG. 2. **Kinetic and polymer energy spectra.** (A) to (F): Energy spectra for different Deborah numbers showing how the elastic range changes with De . (G) and (H): Compensated kinetic energy spectra showing the emergence of two scaling regions, Kolmogorov ($-5/3$) and elastic (-2.3) scaling respectively. In all the previous panels, the dashed and solid lines represent the $-5/3$ and -2.3 scalings. (I): Compensated polymer energy spectra for different Deborah numbers. The solid line represent the scaling $k^{-\psi}$ with $\psi \approx 1.35$. The scaling laws in (G–I) extend over the scales found from the cross overs extracted from Fig. (3). The abscissa are normalized with the integral length scale wavenumber k_L .

over the wavenumber range $k_p < k < k_\eta$. The elastic range spans over the maximum range of wavenumber for $De \approx 1$; as De is increased further the elastic range begins to shrink and the Kolmogorov range begins to grow again. Eventually, the elastic range practically disappears at $De \approx 5$ – the classical Kolmogorov range is restored. This remarkable behavior is better elucidated by plotting the two compensated spectra $k^{5/3}E(k)$ and $k^\xi E(k)$ in Fig. (2G) and Fig. (2H), respectively. In other words, our results clearly show that the wavenumber k_p depends non-monotonically on the Deborah number, being maximum for $De \approx 1$. The non-monotonic behaviour of the polymeric flow for $De \approx 1$ can be also qualitatively appreciated by observing Fig. (1).

Although, the steepening of the spectra beyond a certain wavenumber $k = k_p$ have been observed before in both direct numerical simulations [9, 11, 18, 19, 27] and experiments [33], this was mostly confined to the dissipation range due to the small separation of scales related to the Reynolds number considered; only recent experiments [1], demonstrated for the first time the emergence of this elastic scaling. Ref. [1] also found that L_p increases with the polymer concentration but they did not investigate how it behaves as a function of the Deborah number. Also, we find for the first time both Kolmogorov and elastic scaling simultaneously valid for different ranges of wavenumbers by virtue of running the largest simulation of polymeric turbulence so far and we also uncover the non-monotonic behavior of L_p as a function of the Deborah number. We have also confirmed that these results are robust with respect to change in spatial and temporal resolutions, see Fig. (S2).

The previous results have been obtained for the purely elastic Oldroyd-B model. Before we explore further the elastic scaling, it is worth mentioning that we performed the simulation for $De \approx 0.95$ with two additional models of polymeric fluids – the inelastic, shear-thinning Carreau Yasuda model and the FENE-P model, which models both the elastic and shear-thinning behaviour of polymeric fluids. We find that the new scaling at intermediate scales is a purely elastic effect, which completely disappear in the absence of elasticity, while it is reduced when shear-thinning

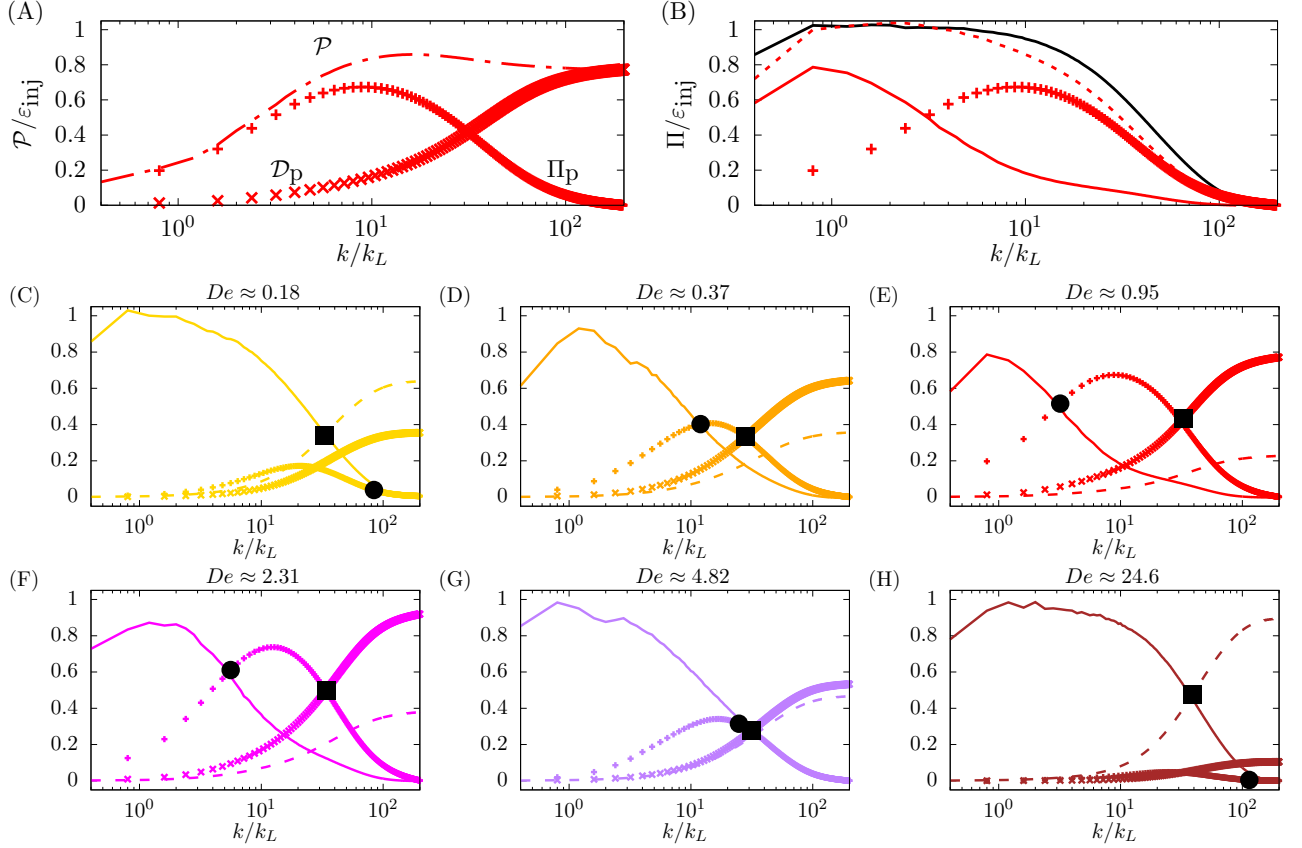


FIG. 3. **Scale by scale energy budget** (A): The polymer contribution to the spectral energy balance, \mathcal{P} , (dash-dotted line) is decomposed into a (\times) pure polymer dissipation term, \mathcal{D}_p and a (+) pure polymer energy flux, Π_p , see (8a). (B): The sum of the (solid line) non-linear energy flux Π_f and of the (+) polymer flux Π_p provide a (dotted line) total flux $\Pi = \Pi_f + \Pi_p$ extending over a range comparable to the Newtonian case (black line). (C) to (H): The panels show the non-linear energy flux Π_f (solid line), fluid dissipation \mathcal{D}_f (dashed line), polymer flux, Π_p (+), and polymer dissipation \mathcal{D}_p (\times) for different Deborah numbers. The filled circles represent k_p and the filled squares k_η , used in Fig. (2G–I) as the extension of the scaling laws. As De approaches unity, the polymer flux and dissipation grow, while they decrease for larger values. The abscissa are normalized with the integral length scale wavenumber k_L . The color scheme is the same used in Fig. (2).

is present together with elasticity (see Fig.(S3) in the Supplementary Materials). We have also observed that if the parameter \mathcal{L} (the maximum possible extension of the polymers) of the FENE-P model is varied within a reasonable range the elastic scaling remains practically unchanged. For too small a value of \mathcal{L} the elastic scaling range can disappear, see Fig. (S3B).

D. Scale-by-scale energy budget

In turbulence, to understand the energy spectra we have to study the flux of energy through scales [46, 50, 51]. For polymeric turbulence, the flux in Fourier space have been studied before by Refs. [26, 27] and their real space analog in Ref. [18].

To obtain the flux of kinetic energy in Fourier space, transform (1a) to Fourier space, multiply by $\hat{u}(-k)$, integrate over the solid angle $d\Omega$ and over k from 0 to K , and average over the statistically stationary state of turbulence to obtain

$$\varepsilon_{\text{inj}} = \varepsilon_f + \varepsilon_p = \Pi_f(K) + \mathcal{D}_f(K) + \mathcal{P}(K) + \mathcal{F}_{\text{inj}}(K), \quad (7)$$

where Π_f , \mathcal{D}_f , \mathcal{P} and \mathcal{F}_{inj} are the contributions from the nonlinear term, the viscous term, the polymeric stress and the external force in (1a) (see the Supplementary Materials for a full derivation). The first equality of (7) follows from statistical stationarity. For $K \gg k_{\text{inj}}$, the external force is zero hence its contribution to the flux, \mathcal{F}_{inj} is constant, i.e.,

$\mathcal{F}_{\text{inj}}(K \gg k_{\text{inj}}) = \varepsilon_{\text{inj}}$. In the absence of polymers, $\mathcal{P} = 0$, and, since in the inertial range the dissipative contribution \mathcal{D}_f is negligible, $\Pi_f(K \gg k_{\text{inj}}) = -\varepsilon_{\text{inj}}$ is a constant. The Kolmogorov four-fifth law follows from this statement [46]. In addition, if we assume that scaling we obtain $E(k) \sim k^{-5/3}$.

The novel physics of this problem is elucidated by studying the contribution from the polymers, \mathcal{P} . In Fig. (3A) we show a representative plot of $\mathcal{P}(K)$ as a function of K , plotted as a dashed-dotted line. It is well established [4, 5, 42] that one of the effects of addition of polymers to flows is the increase of dissipation, but $\mathcal{P}(K)$ is not a purely dissipative term, as shown by its non-monotonicity with K . This feature has been modelled before by a wavenumber dependent effective viscosity [9]. Here we try a different approach. We separate the part of $\mathcal{P}(K)$ which is purely dissipative, $\mathcal{D}_p(K)$, such that at large K such a term should have the same asymptotic dependence on K as $\mathcal{D}_f(K)$. We further demand that as $K \rightarrow \infty$, $\mathcal{D}_p(K) \rightarrow \varepsilon_p$. Hence we obtain:

$$\mathcal{P}(K) = \Pi_p(K) + \mathcal{D}_p(K), \quad \text{where} \quad (8a)$$

$$\mathcal{D}_p(K) \equiv \frac{\varepsilon_p}{\varepsilon_f} \mathcal{D}_f(K). \quad (8b)$$

We plot Π_p and \mathcal{D}_p individually in Fig. (3A). Remarkably, Π_p has the same qualitative behavior as Π_f , the nonlinear flux. In Fig. (3B) we plot both Π_p and Π_f denoted by the symbol + and a continuous line respectively. We find that for small K , Π_f is dominant and Π_p is insignificant. At a certain scale k_* the two fluxes cross each other. Beyond k_* , Π_p is the dominant partner and Π_f is negligible. At very large K , well within the dissipation range, both Π_f and Π_p go to zero. The sum of these two fluxes $\Pi \equiv \Pi_p + \Pi_f$ is practically a constant for all $K \ll k_\eta$. In the same figure, Fig. (3B), we also plot, as a black line, the contribution to the flux from the nonlinear term for a simulation with no polymers. Clearly, the flux that is carried by the nonlinear term in the absence of polymers is carried by both Π_f and Π_p in the presence of polymers: at small K the flux is carried mainly by Π_f and at large K the flux is carried mainly by Π_p . The crossover between this two fluxes happens at k_* which we identify with k_p . The fluxes clearly illustrate and substantiate what we already observed in the energy spectra: for $k < k_p$ the turbulence is Kolmogorov-like whereas for $k_p < k < k_\eta$ the polymeric flux Π_p dominates and is approximately a constant. We define the range of Fourier modes, $k_p < k < k_\eta$ as the *elastic range* with k_p precisely defined as $\Pi_f(k_p) = \Pi_p(k_p)$.

We emphasize, that the decomposition in (8a) and (8b) is justified on the following grounds: first, by construction, $\mathcal{D}_p(K)$ is always positive and monotonically increasing with K ; second, it has the same asymptotic dependence on K as \mathcal{D}_f . While a direct consequence of this decomposition is that $\Pi_p \rightarrow 0$ as $K \rightarrow \infty$, this does not automatically guarantee that net flux $\Pi(K) = \Pi_p(K) + \Pi_f(K)$ is almost a constant over a large range of scales at all De. Our numerical results thus provide an additional post-facto justification of the decomposition of \mathcal{P} . Also, we have checked that other reasonable choices for \mathcal{D}_p do not change the results qualitatively.

For a moment, consider again turbulence without polymers. Assume that within the inertial range, in real space, the velocity shows scaling behavior with an exponent h such that, if we scale length by a factor of b , $x \rightarrow bx$, then velocity scales as $u \rightarrow b^h u$. In the inertial range, the flux equation, (7), implies that the contribution to the flux from the nonlinear term is constant. Applying simple power-counting to the contribution to the flux from the nonlinear term, we obtain $3h - 1 = 0$, which implies the standard result from Kolmogorov theory $h = 1/3$. Let us now apply the same scaling argument to the elastic range [18]. As we scale $x \rightarrow bx$, we expect $u \rightarrow b^h u$, and $C \rightarrow b^g C$ with two distinct exponents h and g , respectively. As the flux Π_p is approximately constant in the elastic range, we obtain $h - 1 + g = 0$. By Fourier transform, it is straightforward to show that, if the velocity in real space scales with an exponent h , then the scaling exponent for the energy, $E(k) \sim k^{-\xi}$, with $\xi = 2h + 1$. Together the two relations imply that the scaling exponent for the shell-integrated polymer energy is $E_p(k) \sim k^{-\psi}$, with $\psi = g + 1 = 2 - (\xi - 1)/2 \approx 1.35$. In Fig. (2I) we plot the compensated shell-integrated polymer spectra from our simulations; a scaling exponent of $\psi \approx 1.35$ is indeed consistent with our results, independently corroborating the view of a polymer flux.

Next, we show how the flux-balance depends on the Deborah number in Fig. (3C-H). We mark two Fourier modes in these plots, one is k_p , marked by a black circle, the wavenumber at which Π_f stops being the dominant contribution, and the other is the wavenumber at which the dissipation (\mathcal{D}_f or \mathcal{D}_p) becomes the dominant term of the balance, which is a reasonable estimate of k_η , marked by a black square. For small De, Fig. (3C), $k_p > k_\eta$; in other words, the elastic range is non-existent, masked by the viscous range. As De increases, Fig. (3D-E), $k_p < k_\eta$ and the elastic range is clearly visible, with k_p reducing with De. As De increases beyond unity, k_p starts increasing again, Fig. (3F), and becomes almost equal to k_η in Fig. (3G). For even larger De, the elastic range disappears again. The values of k_p and k_η obtained from Fig. (3) are used in Fig. (2G-I) as the extension of the scaling laws; the agreement between the two is an independent verification of the validity of (8a) and (8b).

Finally, this non-monotonic behavior of the scale k_p is also reflected in the probability distribution function (PDF) of the squared extension of the polymers, $\text{Tr}(\mathcal{C})$, shown in Fig. (4) for the Oldroyd-B model. For small Deborah numbers, the PDF has a peak somewhat higher than 3, i.e., some polymers are already not in a coiled state. This is expected because the stretching of polymers is determined by the small scale strain-rate [52–54] which is best captured by the Weissenberg number, which is about 16 for the smallest Deborah number we used. As De is increased, the peak

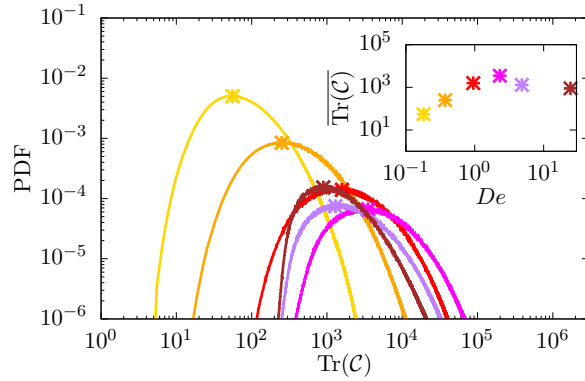


FIG. 4. **Polymer extension.** Probability distribution function (PDF) of the squared extension of the polymer for different Deborah numbers, measured in terms of $\text{Tr}(\mathbf{C})$. The yellow, orange, red, magenta, purple and brown colors are used for increasing values of Deborah numbers, and the color scheme is the same used in Fig. (2). The mean polymer extension (marked with a cross) is a non-monotonic function of the Deborah number, as shown in the inset of the figure.

of the PDF moves to higher and higher values, which is also what is expected. Surprisingly, for $De > 1$ the peak moves back to smaller values. This is an effect that cannot be captured from a passive polymer theory [49] – the feedback from the polymer to the flow changes the strain-rate such that in turn the stretching of the polymers is reversed at Deborah number greater than unity. Note that here we show results from the Oldroyd-B model where there is no constraint on the maximum stretching of polymers; however, this non-monotonic behaviour is not unique to the Oldroyd-B model, and we observe it also with the FENE-P model (see Fig. (S4B) in the Supplementary Materials). Furthermore, since the polymer extension does not continuously increase with the Deborah number, the solution remains effectively dilute also at these high values of Weissenberg numbers, without invalidating the dilute hypothesis of the models used.

To summarize, we have, so far, presented evidence from the largest resolution direct numerical simulations of polymeric turbulence that, if the Deborah number lies in the right range, $k_p < k < k_\eta$, an elastic range with constant polymeric flux Π_p emerges in which $E(k) \sim k^{-\xi}$, with $\xi \approx 2.3$ and $E_p(k) \sim k^{-\psi}$ with $\psi \approx 1.35$. Crucially, the scale k_p behaves non-monotonically as a function of De and can be precisely determined as the cross-over scale between Π_f and Π_p .

E. Structure function and intermittency

In the absence of polymers, the scaling exponents of the structure function ζ_q are a nonlinear function of q – a phenomena known as intermittency [46, Chapter 8], which can be parametrised by corrections to the Kolmogorov scaling

$$\zeta_q = q/3 + \delta_q. \quad (9)$$

The best estimates [55] of δ_q are $\delta_2 \approx 0.04$, $\delta_4 \approx -0.05$, $\delta_6 \approx -0.23$, whereas $\delta_3 = 0$ due to Kolmogorov's four-fifth law. We now explore what happens to intermittency *on the addition of polymers*. In Fig. (5A) we plot the structure function for $q = 2, 4$, and 6 for $De \approx 0.9$ – the case for which we have the largest elastic range. The second order structure function, (3a), with $q = 2$, is the Fourier transform of the energy spectrum $E(k)$. Hence, if $E(k) \sim k^{-\xi}$, then $S_2(\ell) \sim \ell^{\zeta_2}$, with $\zeta_2 = \xi - 1 \approx 1.3$, which is what we obtain. On the other hand, the scalings for $q = 4$ and $q = 6$ are different from $2\zeta_2$ and $3\zeta_2$; this becomes obvious when we plot in Fig. (5B) S_4 and S_6 as a function of S_2 [56]. In these plots the elastic range and the inertial range seems to merge into one scaling range, suggesting that the intermittency correction for $q = 4$ and $q = 6$ are the same in both the elastic and the inertial range. Our results on intermittency discussed so far, agree with the experimental results obtained in Ref. [1]. Thus we must conclude that the effect of the polymers is to change the dominant exponent $q/3$ but not the intermittency correction δ_q ! The dominant exponent is determined by the scaling of the mean value of the energy flux, Π_f , whereas the intermittency exponents are determined by the fluctuations of the energy flux [46, Chapter 8]. The polymers change the mean significantly, but the fluctuations are still dominated by the fluctuations of viscous energy dissipation which remains unchanged on the addition of polymers.

To check this hypothesis we now use an alternative way to explore intermittency: through the statistics of the viscous dissipation. We find that the q -th moment of the viscous dissipation averaged over a ball of radius ℓ shows

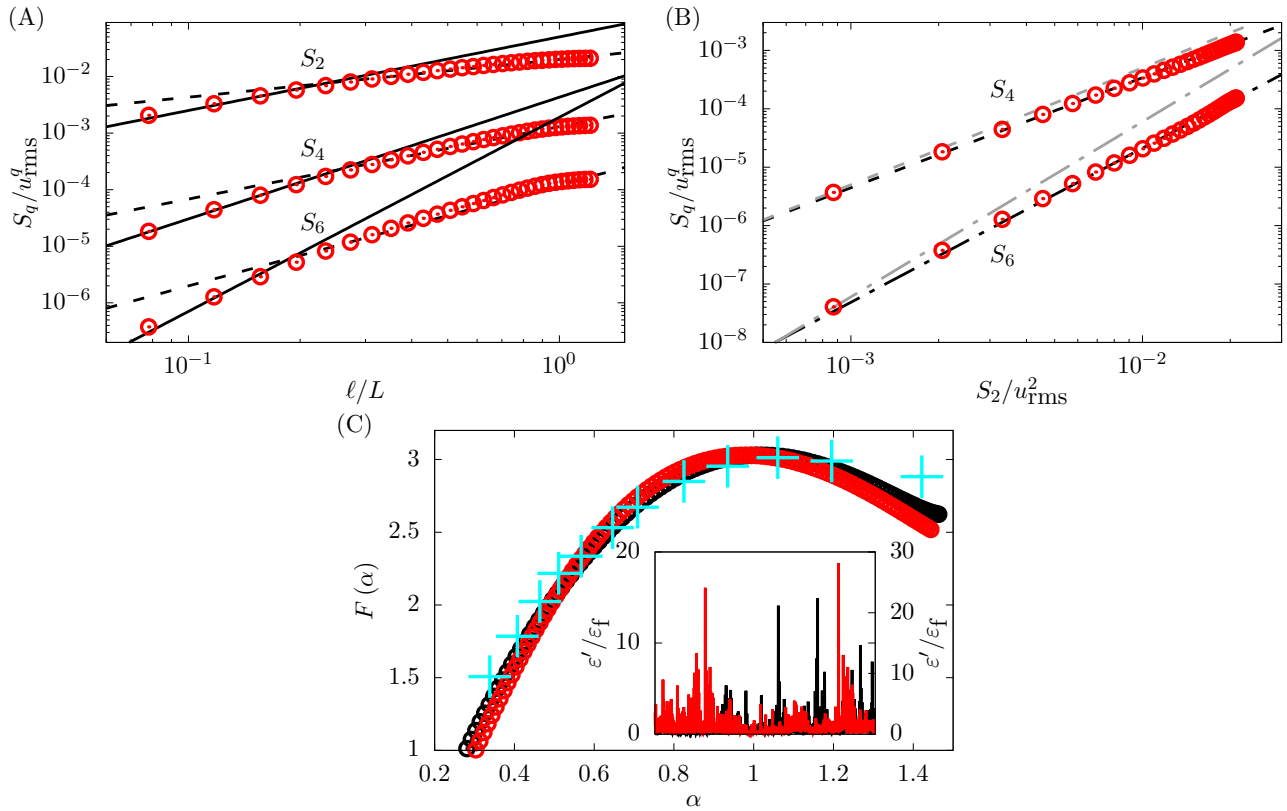


FIG. 5. **Intermittency.** (A): Structure function S_q for $q = 2, 4$ and 6 from top to bottom for the viscoelastic case at $De \approx 0.9$. The solid and dashed lines represent the expected scalings in the polymer and inertial range of scales, corrected by the intermittency correction. (B): Same structure functions of the panel (A), plotted in their Extended Self Similarity form [56]. The black and gray lines represent the expected scaling with and without intermittency corrections. The polymer and inertial range of scales follows the same line, indicating that the intermittency in the two ranges is the same. (C): Multifractal spectrum of the fluid dissipation. The cyan symbols represents experimental data taken from Ref. [57]. The inset shows typical signals for the fluid dissipation, normalized by its mean value. In the two figures, the Newtonian and viscoelastic cases are shown in black and red, respectively.

scaling, viz.,

$$\langle \varepsilon_\ell^q \rangle \sim \ell^{\lambda_q}, \quad \text{where} \quad (10a)$$

$$\varepsilon_\ell \equiv \frac{2\mu_f}{\rho_f} \langle S_{\alpha\beta} S_{\alpha\beta} \rangle_\ell. \quad (10b)$$

Here the symbol $\langle \cdot \rangle_\ell$ denotes averaging over a ball of radius ℓ and the symbol $\langle \cdot \rangle$ averaging over the statistically stationary state of turbulence. For $\ell = L$, $\langle \varepsilon_L \rangle = \varepsilon_f$ the viscous dissipation in (2). The Legendre transform of the function λ_q give the multifractal spectrum of turbulence $F(\alpha)$ which we plot in Fig. (5C). Our results, for the Newtonian case, agrees with the experiments in the Newtonian turbulence [57]. Remarkably, we find that the multifractal spectrum is the same with or without polymers, thereby confirming our hypothesis.

Altogether these evidences point towards the scenario. For small enough viscosity and for small enough k ($k_{inj} < k < k_d$), the energy flux has two contributions – the advective flux and the polymeric flux. In the inertial range the advective flux dominates. In the elastic range the polymeric flux dominates. However the intermittency exponents are determined not by the mean value of the flux but by its fluctuations. The fluctuations are determined by the fluctuations of the viscous dissipation, which remains the same in both polymeric and Newtonian turbulence.

III. DISCUSSION

Our simulations reach the highest Re and De numbers reached so far in numerical simulations of homogeneous and isotropic turbulence of polymer solutions [47]. Hence, by modern nomenclature, we may call this *elasto-inertial*

turbulence [27, 59], which is merely a renaming of the traditional field of polymeric turbulence. We find that the central role of the polymers is that the cascade of energy, which in absence of polymers is determined by the advective nonlinearity, is now carried by both the advective nonlinearity and the polymer stress *but at different scales*. At large scales, the energy flux through scales is dominated by the advective nonlinearity, while the polymer stress plays a sub-dominant role – this is reversed at smaller scales. This gives rise to two scaling ranges, the classical Kolmogorov one and the new elastic one. We emphasize that the new scaling we find is a purely elastic effect, the advective nonlinearity plays a sub-dominant role in the range of scales where the elastic scaling is observed. A comparison of different models of polymeric fluids confirms that elasticity and not shear thinning is crucial to observe the new elastic scaling range in the energy spectrum. Thus elasto-inertial turbulence appears to be inertial turbulence at large scale and a new elastic behaviour – different from elastic turbulence – at smaller scales which are still larger than viscous scales. The viscous effects may dominate over the elastic effects for small Re , thereby making the elastic range disappear. Furthermore, we establish that this elastic behaviour is non-monotonic in Deborah number. A simple qualitative explanation for this effect is that when $De \gg 1$, polymers are not able to properly stretch due to their timescale being much larger than the largest timescale of the fluid, thus acting as a filter of the velocity fluctuations. However, our simulations with passive polymers show that this scenario is not true (polymer extension increases monotonically with De). Thus the non-monotonic behavior observed by us cannot be captured by a theory that treats polymers as passive objects.

At present there are no theories that help us understand the novel scaling. To the best of our knowledge the first theory that predicted a new power-law scaling in elastic range is by Bhattacharjee and Thirumalai [13, 14], whose theory gives an exponent of $\xi = 3$ in the elastic range; by contrast we observe $\xi \approx 2.3$, consistent with recent experiments [1]. Bhattacharjee and Thirumalai also assumed that most of the polymers have not undergone coil-stretch transition. In our simulations, this may be true at small De , where the elastic range is non-existent, but this is definitely not the case at high De where we do observe the elastic scaling. The theory by Fouxon and Lebedev [15] also predicts a power-law scaling ($\xi > 3$) and the existence of an elastic range, but we agree with Zhang et al [1] that “the assumptions and quantitative prediction of the theory are not supported by” our numerics. We believe the elastic range we observe is distinct from elastic turbulence in two ways. One, the scale-dependent Reynolds number in the elastic range is not necessarily very small. Two, we find $\xi \approx 2.3$ whereas almost all study of elastic turbulence find $\xi > 3$ [19, 24, 35, 36, 60, 61], consistent with the theory of Fouxon and Lebedev [15]. Note that, at least one other simulation of elastic turbulence [62] has found $\xi < 3$ in two dimensional polymeric flows.

Our simulations extends the recent experiments by Zhang et. al. [1], who did not probe the Deborah number dependence, by measuring quantities that are not easily accessible in the experiments, e.g., the contribution from the polymeric stress and the PDF of polymer extension, thereby providing constraints and clues to a future theory. We show, for the first time, that the polymer contribution can be decomposed into a purely dissipative term and into a purely energy flux, with the latter transporting the majority of energy in the elastic range. Its validity has been confirmed in several ways: (i) its span is consistent with the range of the elastic scale in the energy spectra; (ii) the polymer energy spectra exhibits a scaling consistent in range and slope with it. Finally, we show that the intermittency corrections are the same in the elastic and the Newtonian cases. This indicates that the statistical nature of the fluctuations of the energy flux remains unchanged on addition of polymers – the fluctuations are determined by the statistics of the viscous energy dissipation, which remains the same in both polymeric and Newtonian turbulence.

IV. MATERIALS AND METHODS

The viscoelastic fluid is governed by the conservation of momentum and the incompressibility constraint:

$$\rho_f \left(\frac{\partial u_\alpha}{\partial t} + \frac{\partial u_\alpha u_\beta}{\partial x_\beta} \right) = -\frac{\partial p}{\partial x_\alpha} + \frac{\partial}{\partial x_\beta} \left(2\mu_f S_{\alpha\beta} + \frac{\mu_p}{\tau_p} f C_{\alpha\beta} \right), \quad (11a)$$

$$\frac{\partial u_\alpha}{\partial x_\alpha} = 0. \quad (11b)$$

In the previous set of equations, ρ_f and μ_f are the density and dynamic viscosity of the fluid, p is the pressure, and \mathcal{S} the rate-of-strain tensor with components $S_{\alpha\beta}$ defined as $S_{\alpha\beta} = (\partial u_\alpha / \partial x_\beta + \partial u_\beta / \partial x_\alpha) / 2$. The last term in the momentum equation is the non-Newtonian contribution, with μ_p being the polymer viscosity, τ_p the polymer relaxation time, f a scalar function and \mathcal{C} the conformation tensor with components $C_{\alpha\beta}$ found by solving the following transport equation:

$$\frac{\partial C_{\alpha\beta}}{\partial t} + u_\gamma \frac{\partial C_{\alpha\beta}}{\partial x_\gamma} = C_{\alpha\gamma} \frac{\partial u_\beta}{\partial x_\gamma} + C_{\gamma\beta} \frac{\partial u_\alpha}{\partial x_\gamma} - \frac{f C_{\alpha\beta} - \delta_{\alpha\beta}}{\tau_p}. \quad (12)$$

The function f is equal to $f = 1$ in the purely elastic Oldroyd-B model, and to $f = (\mathcal{L}^2 - 3) / (\mathcal{L}^2 - C_{\gamma\gamma})$ in the FENE-P model (\mathcal{L} is the maximum polymer extensibility) exhibiting both shear-thinning and elasticity. Turbulence is sustained by an additional forcing in the momentum equation; in particular, we use the spectral scheme by Eswaran and Pope [45] to randomly injecting energy within a low-wavenumber shell with $1 \leq k \leq 2$.

The equations of motion are solved numerically within a periodic cubic domain box of length 2π , discretized with $N = 1024$ grid points per side with a uniform spacing in all directions, resulting in a total number of around 1 billion grid points. The grid resolution k_{\max} used in the present work is the largest used for viscoelastic fluids and is sufficient to represent all the relevant quantities of interest till the Kolmogorov length-scale η ($k_{\max}\eta \approx 1.7$) [50]. Furthermore, the smallest temporal scale of the flow, i.e. the Kolmogorov time-scale τ_η , is overly resolved (by two order of magnitude $\tau_\eta/\Delta t \approx 600$), due to stability constraint arising from the non-Newtonian features of the flow, strongly increasing the computational cost. We have confirmed that these results are robust with respect to change in spatial and temporal resolutions, as reported in Fig. (S2) where the energy spectra obtained by different time and space resolutions are compared, finding the robustness of the reported results. To solve the problem, we use the flow solver *Fujin*, an in-house code, extensively validated and used in a variety of problems [63–69], based on the (second-order) finite-difference method for the spatial discretization and the (second-order) Adams-Bashforth scheme for time marching. See also <https://groups.oist.jp/cffu/code> for a list of validations. The non-Newtonian stress equation is solved following the (exact) log-conformation approach [70] to ensure the positive-definiteness of the tensor even at high De , without the addition of any artificial stabilising terms.

V. REFERENCES AND NOTES

-
- [1] Yi-Bao Zhang, Eberhard Bodenschatz, Haitao Xu, and Heng-Dong Xi, “Experimental observation of the elastic range scaling in turbulent flow with polymer additives,” *Science Advances* **7**, eabd3525 (2021).
 - [2] B. Toms, in *Proceedings of First International Congress on Rheology, Volume II* (North-Holland, Amsterdam, 1949) p. 135.
 - [3] M. Tabor and P.G. De Gennes, “A cascade theory of drag reduction,” *Europhys. Lett.* **2**, 519–522 (1986).
 - [4] E.J. Hinch, “Mechanical models of dilute polymer solution in strong flows,” *Phys. Fluids*. **20**, S22 (1977).
 - [5] J.L. Lumley, “Drag reduction in turbulent flow by polymer additives,” *J. Polymer Sci* **7**, 263–290 (1973).
 - [6] D. Bonn, Y. Couder, P.H.J. van Dam, and S. Douady, “From small scales to large scales in three-dimensional turbulence: The effect of diluted polymers,” *Phys. Rev. E* **47**, R28 (1993).
 - [7] Eric van Doorn, Christopher M White, and KR Sreenivasan, “The decay of grid turbulence in polymer and surfactant solutions,” *Physics of Fluids* **11**, 2387–2393 (1999).
 - [8] C Kalelkar, R Govindarajan, and R Pandit, “Drag reduction by polymer additives in decaying turbulence,” *Phys. Rev. E* **72**, 017301 (2004).
 - [9] Prasad Perlekar, Dhrubaditya Mitra, and Rahul Pandit, “Manifestations of drag reduction by polymer additives in decaying, homogeneous, isotropic turbulence,” *Phys. Rev. Lett.* **97**, 264501 (2006).
 - [10] P. Perlekar, *Numerical Studies of three dimensional turbulence with polymer additives and two dimensional turbulence in thin films.*, Ph.D. thesis, Indian Institute of Science, Bangalore, India (2009).
 - [11] Prasad Perlekar, Dhrubaditya Mitra, and Rahul Pandit, “Direct numerical simulations of statistically steady, homogeneous, isotropic fluid turbulence with polymer additives,” *Phys. Rev. E* **82**, 066313 (2010).
 - [12] W-H Cai, F-C Li, and H-N Zhang, “Dns study of decaying homogeneous isotropic turbulence with polymer additives,” *Journal of Fluid Mechanics* **665**, 334–356 (2010).
 - [13] JK Bhattacharjee and D Thirumalai, “Drag reduction in turbulent flows by polymers,” *Physical review letters* **67**, 196 (1991).
 - [14] D Thirumalai and JK Bhattacharjee, “Polymer-induced drag reduction in turbulent flows,” *Physical Review E* **53**, 546 (1996).
 - [15] A. Fouxon and V. Lebedev, “Spectra of turbulence in dilute polymer solutions,” *Phys. Fluids*. **15**, 2060 (2003).
 - [16] T. Vaithianathan and L.R. Collins, “Numerical approach to simulating turbulent flow of a viscoelastic polymer solution,” *Journal of Computational Physics* **187**, 1–21 (2003).
 - [17] R. Benzi, E. De Angelis, R. Govindarajan, and I. Procaccia, “Shell model for drag reduction with polymer additives in homogeneous turbulence,” *Phys. Rev. E* **68**, 016308 (2003).
 - [18] E De Angelis, CM Casciola, R Benzi, and R Piva, “Homogeneous isotropic turbulence in dilute polymers,” *Journal of Fluid Mechanics* **531**, 1–10 (2005).
 - [19] S Berti, A Bistagnino, Guido Boffetta, A Celani, and S Musacchio, “Small-scale statistics of viscoelastic turbulence,” *EPL (Europhysics Letters)* **76**, 63 (2006).

- [20] T. Peters and J. Schumacher, “Two-way coupling of fene dumbbells with a turbulent shear flow.” *Phys. Fluids* **19**, 065109 (2007).
- [21] Filippo De Lillo, Guido Boffetta, and Stefano Musacchio, “Control of particle clustering in turbulence by polymer additives,” *Physical Review E* **85**, 036308 (2012).
- [22] Takeshi Watanabe and Toshiyuki Gotoh, “Hybrid eulerian–lagrangian simulations for polymer–turbulence interactions,” *Journal of Fluid Mechanics* **717**, 535–575 (2013).
- [23] Mani Fathali and Saber Khoei, “Spectral energy transfer in a viscoelastic homogeneous isotropic turbulence,” *Physics of Fluids* **31**, 095105 (2019).
- [24] Takeshi Watanabe and Toshiyuki Gotoh, “Power-law spectra formed by stretching polymers in decaying isotropic turbulence,” *Physics of Fluids* **26**, 035110 (2014).
- [25] M Quan Nguyen, Alexandre Delache, Serge Simoëns, Wouter JT Bos, and Mamoud El Hajem, “Small scale dynamics of isotropic viscoelastic turbulence,” *Physical Review Fluids* **1**, 083301 (2016).
- [26] PC Valente, CB Da Silva, and FT Pinho, “The effect of viscoelasticity on the turbulent kinetic energy cascade,” *Journal of fluid mechanics* **760**, 39–62 (2014).
- [27] PC Valente, CB da Silva, and FT Pinho, “Energy spectra in elasto-inertial turbulence,” *Physics of Fluids* **28**, 075108 (2016).
- [28] C. Friehe and W. Schwarz, *J. Fluid. Mech* **44**, 173 (1970).
- [29] W. McComb, J. Allan, and C. Greated, *Phys. Fluid* **20**, 873 (1977).
- [30] D. Bonn, Y. Amarouchene, C. Wagner, S. Douady, and O. Cadot, “Turbulent drag reduction by polymers,” *J. Phys. CM* **17**, S1219 (2005).
- [31] A. Liberzon, M. Guala, W. Kinzelbach, and A. Tsinober, *Phys. Fluids*. **18**, 125101 (2006).
- [32] N.T. Ouellette, H. Xu, and E. Bodenschatz, “Bulk turbulence in dilute polymer solutions,” *J. Fluid Mech.* **629**, 375–385 (2009).
- [33] Richard Vonlanthen and Peter A Monkewitz, “Grid turbulence in dilute polymer solutions: Peo in water,” *Journal of Fluid Mechanics* **730**, 76–98 (2013).
- [34] LD Landau and EM Lifshitz, *Fluid mechanics*, Course of Theoretical Physics, Vol. 6 (Pergamon Press Ltd., Oxford, England, 1959).
- [35] Alexander Groisman and Victor Steinberg, “Elastic turbulence in a polymer solution,” *Nature* **405**, 53 (2000).
- [36] Victor Steinberg, “Elastic turbulence: an experimental view on inertialess random flow,” *Annual Review of Fluid Mechanics* **53**, 27–58 (2021).
- [37] Heng-Dong Xi, Eberhard Bodenschatz, and Haitao Xu, “Elastic energy flux by flexible polymers in fluid turbulence,” *Physical review letters* **111**, 024501 (2013).
- [38] John L Lumley, “Drag reduction by additives,” *Annual review of fluid mechanics* **1**, 367–384 (1969).
- [39] A. Peterlin, *J. Polym. Sci., Polym. Lett.* **4**, 287 (1966).
- [40] H. Warner, *Ind. Eng. Chem. Fundamentals* **11**, 379 (1972).
- [41] R. Armstrong, *J. Chem. Phys.* **60**, 724 (1974).
- [42] R. Bird, C. Curtiss, R. Armstrong, and O. Hassager, *Dynamics of Polymeric Liquids* (Wiley, New York, 1987).
- [43] N. Phan-Thien, *Understanding Viscoelasticity* (Springer, Berlin, 2002).
- [44] P S Virk, “Drag reduction fundamentals,” *AIChE Journal* **21**, 625–656 (1975).
- [45] Vinayak Eswaran and Stephen B Pope, “An examination of forcing in direct numerical simulations of turbulence,” *Computers & Fluids* **16**, 257–278 (1988).
- [46] U. Frisch, *Turbulence the legacy of A.N. Kolmogorov* (Cambridge University Press, Cambridge, 1996).
- [47] This expression is correct for the Oldroyd-B model, but not for FENE-P model; for the latter, the correct expression can be found in Ref. [48].
- [48] Nusret Balci, Becca Thomases, Michael Renardy, and Charles R Doering, “Symmetric factorization of the conformation tensor in viscoelastic fluid models,” *Journal of Non-Newtonian Fluid Mechanics* **166**, 546–553 (2011).
- [49] R. Benzi and E.S.C. Ching, *Rev. Mod. Phys.* **9**, 163 (2018).
- [50] S B Pope, *Turbulent flows* (Cambridge University Press, 2001).
- [51] Mahendra K Verma, *Energy transfers in fluid flows: multiscale and spectral perspectives* (Cambridge University Press, 2019).
- [52] Michael Chertkov, “Polymer stretching by turbulence,” *Physical review letters* **84**, 4761 (2000).
- [53] M Martins Afonso and D Vincenzi, “Nonlinear elastic polymers in random flow,” *Journal of Fluid Mechanics* **540**, 99–108 (2005).
- [54] Stefano Musacchio and Dario Vincenzi, “Deformation of a flexible polymer in a random flow with long correlation time,” *Journal of fluid mechanics* **670**, 326–336 (2011).
- [55] Katepalli R Sreenivasan and Brindesh Dhruva, “Is there scaling in high-reynolds-number turbulence?” *Progress of Theoretical Physics Supplement* **130**, 103–120 (1998).
- [56] R Benzi, S Ciliberto, R Tripiccone, C Baudet, F Massaioli, and S Succi, “Extended self-similarity in turbulent flows,” *Physical Review E* **48**, R29 (1993).
- [57] Charles Meneveau and KR Sreenivasan, “The multifractal nature of turbulent energy dissipation,” *Journal of Fluid Mechanics* **224**, 429–484 (1991).
- [58] See supplemental material for a comparisons of our parameters with all the earlier simulations.
- [59] Devranjan Samanta, Yves Dubief, Markus Holzner, Christof Schäfer, Alexander N Morozov, Christian Wagner, and Björn Hof, “Elasto-inertial turbulence,” *Proceedings of the National Academy of Sciences* **110**, 10557–10562 (2013).

- [60] Samriddhi Sankar Ray and Dario Vincenzi, “Elastic turbulence in a shell model of polymer solution,” *EPL (Europhysics Letters)* **114**, 44001 (2016).
- [61] Anupam Gupta and Rahul Pandit, “Melting of a nonequilibrium vortex crystal in a fluid film with polymers: Elastic versus fluid turbulence,” *Physical Review E* **95**, 033119 (2017).
- [62] Anupam Gupta and Dario Vincenzi, “Effect of polymer-stress diffusion in the numerical simulation of elastic turbulence,” *Journal of Fluid Mechanics* **870**, 405–418 (2019).
- [63] M. E. Rosti, Z. Ge, S. S. Jain, M. S. Dodd, and L. Brandt, “Droplets in homogeneous shear turbulence,” *J. Fluid Mech.* **876**, 962–984 (2019).
- [64] M. E. Rosti and L. Brandt, “Increase of turbulent drag by polymers in particle suspensions,” *Phys. Rev. Fluids* **5**, 041301 (2020).
- [65] M. E. Rosti, S. Olivieri, M. Cavaola, A. Seminara, and A. Mazzino, “Fluid dynamics of COVID-19 airborne infection suggests urgent data for a scientific design of social distancing,” *Sci. Rep.* **10**, 1–9 (2020).
- [66] S. Olivieri, L. Brandt, M. E. Rosti, and A. Mazzino, “Dispersed fibers change the classical energy budget of turbulence via nonlocal transfer,” *Phys. Rev. Lett.* **125**, 114501 (2020).
- [67] M. E. Rosti, M. Cavaola, S. Olivieri, A. Seminara, and A. Mazzino, “Turbulence role in the fate of virus-containing droplets in violent expiratory events,” *Phys. Rev. Research* **3**, 013091 (2021).
- [68] A. Mazzino and M. E. Rosti, “Unraveling the secrets of turbulence in a fluid puff,” *Physical Review Letters* **127**, 094501 (2021).
- [69] S. Brizzolara, M. E. Rosti, S. Olivieri, L. Brandt, M. Holzner, and A. Mazzino, “Fiber tracking velocimetry for two-point statistics of turbulence,” *Phys. Rev. X* **11**, 031060 (2021).
- [70] R. Fattal and R. Kupferman, “Constitutive laws for the matrix-logarithm of the conformation tensor,” *Journal of Non-Newtonian Fluid Mechanics* **123**, 281–285 (2004).

VI. ACKNOWLEDGMENTS

M.E.R. thanks Ms. Megumi Ikeda of the Complex Fluids and Flows unit at OIST for the help and useful discussions in preparing the flow visualisation.

A. Funding

M.E.R. is supported by the Okinawa Institute of Science and Technology Graduate University (OIST) with subsidy funding from the Cabinet Office, Government of Japan. M.E.R. also acknowledges the computational time provided by HPCI on the Fugaku cluster under the grants hp210229 and hp220099, and the computer time provided by the Scientific Computing section of Research Support Division at OIST. PP acknowledges support from the Department of Atomic Energy (DAE), India under Project Identification No. RTI 4007, and DST (India) Project Nos. ECR/2018/001135 and DST/NSM/R&D.HPC_Applications/2021/29. DM acknowledges the support of the Swedish Research Council Grant No. 638-2013-9243 and 2016-05225.

B. Author contributions

M.E.R. conceived the original idea, planned the research, developed the code and performed the numerical simulations. All authors analyzed data, outlined the manuscript content and wrote the manuscript.

C. Competing interests

The authors declare that they have no competing interests.

D. Data availability

All data needed to evaluate the conclusions are present in the paper and/or the Supplementary Materials.

The code used for the present research is a standard direct numerical simulation solver for the Navier–Stokes equations. Full details of the code used for the numerical simulations are provided in the Methods section and references therein.

SUPPLEMENTARY INFORMATION

Energy balance equation

We perform the Fourier transform of the governing equations to obtain an expression for the turbulent kinetic energy spectrum $\hat{E}(\boldsymbol{\kappa}, t) \equiv \frac{1}{2}\rho\langle\hat{\mathbf{u}}^* \cdot \hat{\mathbf{u}}\rangle$, where (\cdot) denotes the Fourier transform into the spectral space, $\boldsymbol{\kappa}$ denotes the wave vector with a magnitude κ , and the superscript $*$ denotes the complex conjugate;

$$\boldsymbol{\kappa} \cdot \hat{\mathbf{u}} = 0, \quad (13)$$

$$\rho \frac{d\hat{\mathbf{u}}}{dt} + \hat{\mathbf{G}} = -i\boldsymbol{\kappa}\hat{p} - \mu_f \kappa^2 \hat{\mathbf{u}} + \hat{\mathbf{F}}_{\text{pol}} + \hat{\mathbf{F}}, \quad (14)$$

where $\hat{\mathbf{G}}$ is the Fourier coefficient of the non-linear convective term appearing in the momentum equation, and i is the imaginary unit. Similar equations can be obtained for the complex conjugate $\hat{\mathbf{u}}^*$. When the momentum equation is multiplied by $\hat{\mathbf{u}}^*$, the pressure term $-i\boldsymbol{\kappa} \cdot \hat{\mathbf{u}}^* \hat{p}$ vanishes due to the incompressibility constraint, and the viscous term $-\mu_f \kappa^2 \hat{\mathbf{u}} \cdot \hat{\mathbf{u}}^*$ can be expressed in terms of the kinetic energy; $-2\mu_f \kappa^2 \hat{E}$. The same holds when multiplying the momentum equation of $\hat{\mathbf{u}}^*$ by $\hat{\mathbf{u}}$. By summing the two equations for $\hat{\mathbf{u}}$ and $\hat{\mathbf{u}}^*$ and dividing by 2, we have an expression for the time evolution of turbulent kinetic energy $\hat{E}(\boldsymbol{\kappa}, t)$

$$\frac{d\hat{E}(\boldsymbol{\kappa})}{dt} = \hat{T}(\boldsymbol{\kappa}) + \hat{V}(\boldsymbol{\kappa}) + \hat{F}_{\text{pol}}(\boldsymbol{\kappa}) + \hat{F}(\boldsymbol{\kappa}), \quad (15)$$

where the terms on the right-hand side represent the following contributions: $\hat{T} = -\frac{1}{2}(\hat{\mathbf{G}} \cdot \hat{\mathbf{u}}^* + \hat{\mathbf{G}}^* \cdot \hat{\mathbf{u}})$ is due to the non-linear convective term, $\hat{V} = -2\mu_f \kappa^2 \hat{E}$ is due to the fluid dissipation term, $\hat{F}_{\text{pol}} = \frac{1}{2}(\hat{\mathbf{F}}_{\text{pol}} \cdot \hat{\mathbf{u}}^* + \hat{\mathbf{F}}_{\text{pol}}^* \cdot \hat{\mathbf{u}})$ is due to the non-Newtonian stress, and $\hat{F}_{\text{inj}} = \frac{1}{2}(\hat{\mathbf{F}}_{\text{inj}} \cdot \hat{\mathbf{u}}^* + \hat{\mathbf{F}}_{\text{inj}}^* \cdot \hat{\mathbf{u}})$ is due to the external forcing. The one-dimensional energy spectrum $E(\kappa, t)$ can be obtained by isotropically averaging (15) over the sphere of radius κ (i.e., $E(\kappa, t) = \iint_{S(\kappa)} \hat{E}(\boldsymbol{\kappa}, t) dS(\kappa)$, where $S(\kappa)$ is the sphere defined by $\boldsymbol{\kappa} \cdot \boldsymbol{\kappa} = \kappa^2$),

$$\frac{dE(\kappa)}{dt} = T(\kappa) + V(\kappa) + F_{\text{pol}}(\kappa) + F_{\text{inj}}(\kappa). \quad (16)$$

where the time derivative becomes zero for a statistically stationary flow. Integrating the equation above from κ to infinity, we obtain the energy-transfer balance

$$0 = \Pi_f + \mathcal{D}'_f + \mathcal{P}' + \mathcal{F}_{\text{inj}}, \quad (17)$$

where $\Pi_f(\kappa) \equiv \int_{\kappa}^{\infty} T(\kappa) d\kappa$, $\mathcal{D}'_f(\kappa) \equiv \int_{\kappa}^{\infty} V(\kappa) d\kappa$, $\mathcal{F}_{\text{inj}}(\kappa) \equiv \int_{\kappa}^{\infty} F_{\text{inj}}(\kappa) d\kappa$, and $\mathcal{P}'(\kappa) \equiv \int_{\kappa}^{\infty} F_{\text{pol}}(\kappa) d\kappa$ represent the contributions to the spectral power balance from the non-linear convective, fluid dissipation, turbulence forcing, and non-Newtonian terms, respectively. The fluid dissipation term can be expressed as $\mathcal{D}_f(\kappa) = -\int_0^{\kappa} V(\kappa) d\kappa = \mathcal{D}'_f(\kappa) + \langle \varepsilon_f \rangle$, where $\langle \varepsilon_f \rangle = -\int_0^{\infty} V(\kappa) d\kappa$ is the rate of energy dissipated by the fluid viscosity. Similarly, the non-Newtonian contribution can be written as $\mathcal{P}(\kappa) = -\int_0^{\kappa} F_{\text{pol}}(\kappa) d\kappa = \mathcal{P}'(\kappa) + \langle \varepsilon_p \rangle$, where $\langle \varepsilon_p \rangle = -\int_0^{\infty} F_{\text{pol}}(\kappa) d\kappa$ is the non-Newtonian dissipation rate. Substituting these in the above equation, we obtain the energy balance equation used in the main document.

Total energy budget

The total energy of a FENE-P polymeric fluid system described by the governing equations is given by [18]:

$$F \equiv \underbrace{\frac{1}{2}\langle |u|^2 \rangle}_{\mathcal{E}_f} + \underbrace{\frac{\mu_p}{2\rho_f \tau_p} [\langle (L^2 - 3) \log(f) \rangle + 3]}_{\mathcal{E}_p}, \quad (18)$$

where \mathcal{E}_f is the kinetic energy, and \mathcal{E}_p is the contribution due to the polymer conformation. Note that by taking the limit $L \rightarrow \infty$ we get the corresponding expression for the Oldroyd-B model, $\mathcal{E}_p = (\mu_p/2\rho_f \tau_p) \langle C_{\gamma\gamma} \rangle$. By taking the time-derivative of (18), and using equations (1a), (1b) we get the following energy budget equation

$$\frac{\partial F}{\partial t} = - \underbrace{\frac{2\mu_f}{\rho_f} \langle S_{\alpha\beta} S_{\alpha\beta} \rangle}_{\mathcal{E}_f} - \underbrace{\frac{\mu_p}{2\rho_f \tau_p^2} \langle f(f C_{\mu\mu} - 3) \rangle}_{\mathcal{E}_p}. \quad (19)$$

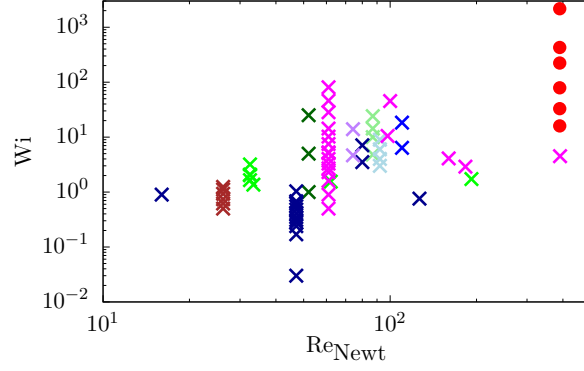


FIG. S1. **DNS data of polymeric turbulence available in the literature.** The plot reports the reference Reynolds numbers of the Newtonian cases Re_{Newt} and the Weissenberg numbers Wi of the simulations available in the literature: the cross symbols represents the previous investigations, while the filled circles the present one. Light green: Berti *et al.* [19]; green: Nguyen *et al.* [25]; dark-green: Watanabe and Gotoh [22, 24]; light blue: Fathali and Khoei [23]; blue: De Lillo *et al.* [21]; dark blue: Perlekar *et al.* [9, 11]; magenta: Valente *et al.* [26, 27]; purple: De Angelis *et al.* [18]; brown: Cai *et al.* [12]. The results of the present work focus on a high Re and Wi region never investigated before.

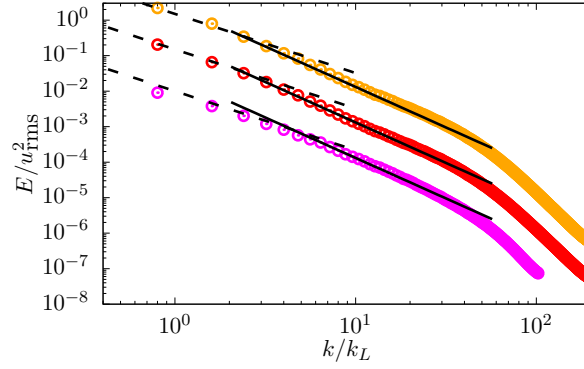


FIG. S2. **Numerical resolution.** Energy spectra for $De \approx 0.95$ obtained by (orange) reducing the timestep by a factor 10 and by (magenta) reducing the grid size by a factor 2. The spectra are shifted vertically for visual clarity. In both cases, the grid and time resolution proves to be appropriate.

Elasticity and shear-thinning

We consider three different models of polymeric fluids: the Oldroyd-B model (elasticity), the FENE-P model (elasticity and shear-thinning), and the Carreau-Yasuda model (shear-thinning), see Tab. S1 for the full list of simulations performed. In the inelastic shear-thinning fluid, the fluid viscosity μ_f is a function of the local shear rate $\dot{\gamma}$ as

$$\frac{\mu}{\mu_0} = \frac{\mu_\infty}{\mu_0} + \left(1 - \frac{\mu_\infty}{\mu_0}\right) \left[1 + (\tau_p \dot{\gamma})^2\right]^{\left(\frac{n-1}{2}\right)}, \quad (20)$$

where μ_0 and μ_∞ are the viscosity at zero and infinite shear rates, n is the power index ($n = 0.4$) and τ_p the consistency index. The model parameters are found to fit the FENE-P shear-thinning rheology, as shown in the inset of Fig. (S3A).

When comparing the results obtained for different non-Newtonian models, we find that the new power-law scaling in the energy spectra at intermediate small scales is a purely elastic effect, which completely disappear in the absence of elasticity while it is slightly reduced in range when shear-thinning is present together with elasticity, as shown in Fig. (S3A). When both elasticity and shear-thinning effects are present, the exponent of the power-law scaling remains practically unchanged if the parameter \mathcal{L} (the maximum possible extension of the polymers) of the FENE-P model is varied within a reasonable range, while the elastic scaling range can completely disappear for too small values, showing a complex behaviour. While the presence of shear-thinning in combination with elasticity does not alter the

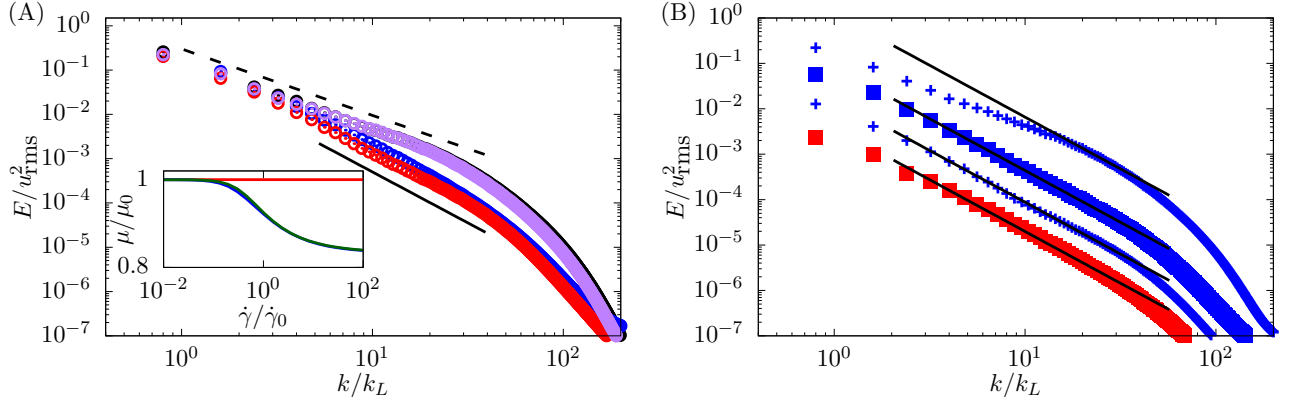


FIG. S3. **Effect of shear-thinning and elasticity on the energy spectra.** (A): Energy spectra for $De \approx 0.95$ for different fluids. Black: Newtonian fluid. Purple: inelastic Carreau Yasuda model. Blue: FENE-P model. Red: Oldroyd-B model. The inset shows the shear rheology of the same fluids. The new scaling at intermediate small scales is a purely elastic effect, which completely disappear in the absence of elasticity while it is reduced when shear-thinning is present together with elasticity. (B): Energy spectra for $De \approx 0.95$ for FENE-P fluids with different \mathcal{L} . From top to bottom: $\mathcal{L} = 20, 60, 100, \infty$ (Oldroyd-B model). The spectra in the right panel are shifted vertically for visual clarity. The new scaling at intermediate small scales is present for all cases with sufficiently large \mathcal{L} . The dashed and solid lines represent the scaling $k^{-\psi}$ with $\psi = 5/3$ and $\psi \approx 1.35$.

slope of the elastic range, it reduces its range: this is caused by an enhancement of the non-linear energy flux Π_f and a consequent reduction of the polymer flux, Π_p , as shown in Fig. (S4A). In the FENE-P model the extension of the polymers is arrested due to two mechanisms. One because of the feedback to the flow, and two because of the nonlinear saturation term in the FENE-P equation itself. If \mathcal{L} is small, the nonlinear saturation term stops the polymers from having large extensions. This implies that the feedback from the polymer to the flow is also small, consequently the flux Π_p is also small. Hence, as \mathcal{L} is increased, Π_p increases and Π_f decreases. When $\mathcal{L} \rightarrow \infty$, which corresponds to the Oldroyd-B model, we get the largest possible values for Π_p . In this case the elastic range is best observed.

TABLE S1. List of all cases considered in the present work.

case	model	Re_λ	De	Wi	$\mu_p/(\mu_p + \mu_f)$	\mathcal{L}
○	single phase	390	—	—	0.1	—
◊	Oldroyd-B	480	0.18	16	0.1	∞
◊	Oldroyd-B	630	0.37	33	0.1	∞
○	Oldroyd-B	740	0.95	79	0.1	∞
△	Oldroyd-B	690	2.31	223	0.1	∞
▽	Oldroyd-B	614	4.82	427	0.1	∞
□	Oldroyd-B	447	24.6	2169	0.1	∞
+	FENE-P	420	0.95	79	0.1	20
○	FENE-P	610	0.95	79	0.1	60
×	FENE-P	700	0.95	79	0.1	100
○	FENE-P	620	2.31	31	0.1	60
○	FENE-P	487	4.82	31	0.1	60
○	Carreau-Yasuda	370	—	—	—	—

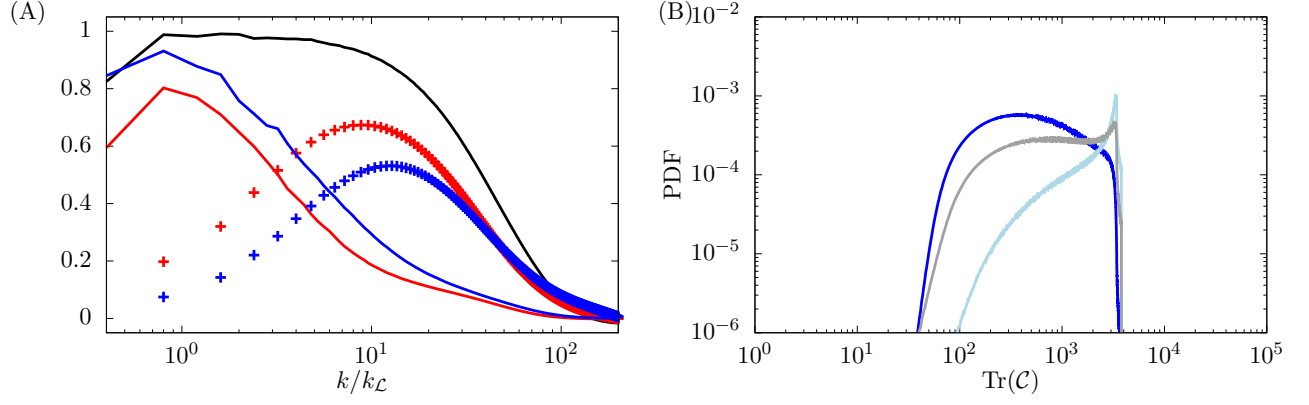


FIG. S4. **Effect of shear-thinning on the energy balance and polymer extension.** (A): the non-linear energy flux Π_f (solid line) and polymer flux, Π_p (+) for the (black) Newtonian, (red) Oldroyd-B and (blue) FENE-P fluids at $De \approx 1$. In the FENE-P fluid, the non-linear energy flux is stronger than in the Oldroyd-B case, resulting in a reduced polymer flux. (B): Probability distribution function (PDF) of the polymer extension for different Deborah numbers, measured in terms of $\text{Tr}(\mathcal{C})$, obtained with the FENE-P model. Blue: $De \approx 0.95$; light blue: $De \approx 2.31$; gray: $De \approx 4.82$. Differently from the results obtained with the Oldroyd-B model, the polymer extension is upper bounded by \mathcal{L}^2 ; however, the non-monotonic trend with De is still evident.